Chapter 5

Michael Kaschke, Karl-Heinz Donnerhacke
and Michael Stefan Rill

Layout by Kerstin Willnauer

Determination of the Refractive Status of the Eye

Solutions to Problems in „Optical Devices in Ophthalmology and Optometry“

Contents

P5.1
Retinoscope

1. Show that the accuracy of a retinoscope can be determined by the equation

$$\Delta\mathcal{D} = \mp \frac{\lambda}{d^2{}_{\mathrm{pupil}}} \quad . \tag{5.38}$$

2. Derive the Newton formula

$$z \cdot z' = f_{\mathrm{L}} \cdot f'_{\mathrm{L}} \tag{5.39}$$

from the thin lens equation (A12).

Solution:

1. According to Eqs. (2.14) or (6.13), the diffraction limited depth of field Δz_{dof} is given by

$$\Delta z_{\mathrm{dof}} = \frac{\lambda}{2 \cdot \mathrm{NA}^2} \quad . \tag{S5.1}$$

In retinoscopy, the depth of field Δz_{dof} determines the localizability of the red reflex within the pupil plane and thereby the principle accuracy of the observer's viewing distance L_{wd}. A change of the working distance within the depth of field Δz_{dof} does not result in any change of the light/shadow-boundary of the red-reflex within the pupil plane. Using the working distance L_{wd} and the pupil diameter of the patient's eye d_{pupil}, we have

$$\mathrm{NA} = \frac{d_{\mathrm{pupil}}}{2 \cdot L_{\mathrm{wd}}}$$

from which we obtain with Eq. (S5.1)

$$\Delta z_{\mathrm{dof}} = \frac{2 \cdot \lambda \cdot L^2_{\mathrm{wd}}}{d^2_{\mathrm{pupil}}} \quad . \tag{S5.2}$$

If we are only concerned about the $\pm$ depth variation from the ideal median position and denote the derivation by ΔL_{wd}, we have

$$\Delta L_{\mathrm{wd}} = \pm \frac{\Delta z_{\mathrm{dof}}}{2} = \pm \frac{\lambda \cdot L^2_{\mathrm{wd}}}{d^2_{\mathrm{pupil}}} \quad . \tag{S5.3}$$

According to Eq. (5.1), a working distance L_{wd} (in m) corresponds to a refractive power of

$$\mathcal{D} = \frac{1}{\Delta L_{\mathrm{wd}}} \quad .$$

Thus, a change in the working distance ΔL_{wd} results in a refractive power change of

$$\Delta\mathcal{D} = -\frac{\Delta L_{\mathrm{wd}}}{L^2_{\mathrm{wd}}}$$

and with ΔL_{wd} from Eq. (S5.3)

$$\Delta\mathcal{D} = \mp\frac{\lambda}{d_{\mathrm{pupil}}^2} \ .$$

A more thorough treatment, which includes a derivation of Eq. (S5.1), is given in the appendix to this problem.

2. The thin lens equation (A12) reads

$$\frac{1}{s'} - \frac{1}{s} = \frac{n'-n}{n} \cdot \left(\frac{1}{r_1} - \frac{1}{r_2}\right) \ .$$

Based on the definition of the focal length, when the object is at optical infinity ($s \to \infty$), the image location indicates the focal length ($s' = f'$), therefore

$$\frac{1}{s'\big|_{s\to\infty}} = \frac{1}{f'} = \frac{n'-n}{n} \cdot \left(\frac{1}{r_1} - \frac{1}{r_2}\right) \ .$$

Correspondingly, we obtain in the case of an image at optical infinity

$$\frac{1}{s\big|_{s'\to\infty}} = \frac{1}{f} = \frac{n'-n}{n} \cdot \left(\frac{1}{r_1} - \frac{1}{r_2}\right)$$

and therefore

$$f = -f' \ . \tag{S5.4}$$

The lens equation can now be written as

$$\frac{1}{s'} - \frac{1}{s} = \frac{1}{f'} \ . \tag{S5.5}$$

From Figure A6, we can derive the simple relations

$$\begin{aligned} s' &= f' + z' \ , \\ s &= f + z \ . \end{aligned} \tag{S5.6}$$

Insertion of Eq. (S5.6) into (S5.5) finally leads to

$$\begin{aligned} &\frac{1}{f'+z'} - \frac{1}{f+z} = \frac{1}{f'} \\ \Rightarrow\ & f' \cdot \big(f + z - (f' + z')\big) = (f+z)\cdot(f'+z') \\ \Rightarrow\ & zz' = -f'^2 - z'(f+f') \ . \end{aligned}$$

Because of Eq. (S5.4), we finally get

$$zz' = f_L \cdot f_L' \ ,$$

where we used the index "L" for the lens.

Appendix to Problem P5.1

We provide here a more thorough treatment of the accuracy of the retinoscope including the derivation of the depth of focus. The measuring accuracy of the retinoscope is related to the depth of focus $2\Delta z$. In the wave optical approximation

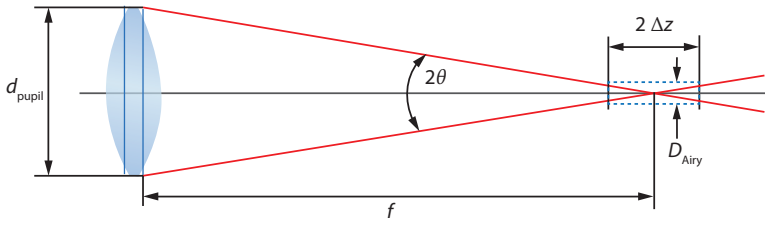

Figure S5.1 Geometry of optical system for the derivation of the retinoscope accuracy.

and in the case of a diffraction-limited imaging quality, the calculations for the depth of focus can be performed as follows:
The (Fraunhofer approximated) diffraction integral reads in circular coordinates for rotational symmetry

$$E(r', z) = N \int E(r) \cdot J_0 \left(\frac{2\pi r r'}{\lambda f} \right) r \mathrm{d}r$$

and in a system with a lens with focal length f

$$E(r') = N \int E_0 \cdot \exp \left(\frac{i\pi r^2}{\lambda f} \right) \cdot J_0 \left(\frac{2\pi r r'}{\lambda f} \right) r \mathrm{d}r \ .$$

With reference distance z and the corresponding defocus term, we obtain

$$E(r', z) = N \int E_0 \cdot \exp \left(\frac{i\pi r^2}{\lambda f} \right) \cdot \exp \left(-\frac{i\pi r^2}{\lambda z} \right) \cdot J_0 \left(\frac{2\pi r r'}{\lambda f} \right) r \mathrm{d}r \ .$$

On the optical axis, we have $r' = 0$ so that

$$E(0, z) = N \int_0^{d_{\mathrm{pupil}}/2} E_0 \cdot \exp \left(\frac{i\pi r^2}{\lambda f} \right) \cdot \exp \left(-\frac{1\pi r^2}{\lambda z} \right) r \mathrm{d}r \ .$$

With the approximation for a small defocus value, that is, a small deviation from the focal plane

$$\frac{1}{z} - \frac{1}{f} \approx \frac{\Delta z}{f^2} \ ,$$

we get

$$E(0,z) = N \int_0^{d_{\mathrm{pupil}}/2} E_0 \cdot \exp\left(\frac{i\pi\Delta z r^2}{\lambda f^2}\right) \cdot r\mathrm{d}r \ .$$

With the standard integral

$$\int_0^b e^{-a^2 r^2} r\mathrm{d}r = \frac{1}{a^2} \cdot \left(1 - e^{-a^2 b^2}\right) \ ,$$

we obtain

$$E(0,\Delta z) = N \cdot E_0 \, \frac{\lambda f^2}{\pi i \, d_{\mathrm{pupil}}^2 \, \Delta z} \cdot \left[1 - \exp\left(-\frac{\pi i \, d_{\mathrm{pupil}}^2 \, \Delta z}{\lambda f^2}\right)\right] \ .$$

Using the abbreviation (scaled axial coordinate according to Wolf)

$$u = \frac{2\pi}{\lambda} \cdot n^2 \cdot \Delta z \cdot \sin^2\theta = \frac{2\pi n \, d_{\mathrm{pupil}}^2 \, \Delta z}{4\lambda f^2} = \frac{2\pi \cdot n\Delta z}{R_{\mathrm{u}}}$$

and the Rayleigh range

$$R_{\mathrm{u}} = \frac{\lambda}{n \cdot \sin^2\theta} = \frac{4f^2\lambda}{n \cdot d_{\mathrm{pupil}}^2}$$

(assuming in paraxial approximation small angles so that $\sin\theta = d_{\mathrm{pupil}}/(2f)$), it follows that

$$E(0,u(\Delta z)) = \overline{E}_0 \frac{1}{iu} \cdot \left(1 - \mathrm{e}^{-\frac{iu}{2}}\right) \ .$$

When calculating of the intensity

$$I(0,u(\Delta z)) = E^*(0,u(\Delta z)) \cdot E(0,u(\Delta z))^n$$

with

$$\cos(ax) = \frac{\mathrm{e}^{iax} + \mathrm{e}^{-iax}}{2} \ ,$$

we obtain with $u = u(\Delta z)$

$$I(0,u(\Delta z)) = I_0 \cdot \frac{\sin(u/4)}{(u/4)^2} = I_0 \ \mathrm{sinc}^2\left(\frac{u}{4}\right) \ .$$

Thus, in the case of defocussing, the intensity decreases according to the sinc-functions (Figure S5.2). If we defocus in a way that the normalized intensity $I(\Delta z) = I_0$ reaches a value of 80 % (corresponding to the Rayleigh criterion for diffraction limit), we obtain the half interval for the optical depth of focus

$$\begin{aligned}\Delta z_f &= \frac{u}{2\pi} \cdot R_{\mathrm{u}} = \frac{u}{4} \cdot \frac{2}{\pi} \cdot R_{\mathrm{u}} \\ &= 0.80091 \cdot \frac{2}{\pi} \cdot R_{\mathrm{u}} = \frac{0.5150 \cdot \lambda}{n' \cdot \sin^2\theta} \\ &\approx \frac{\lambda}{2n' \cdot \sin^2\theta} = \frac{R_{\mathrm{u}}}{2} = \frac{2f^2\lambda}{d_{\mathrm{pupil}}^2} \ .\end{aligned}$$

In reality, a smaller decrease of the intensity by 20% can be detected by the human eye. Therefore, one usually assumes half the defocus as detectable

$$\Delta z_f = \frac{R_\mathrm{u}}{4} = \frac{f^2\lambda}{d^2_\mathrm{pupil}} \quad . \tag{S5.7}$$

In retinoscopy, the refractive power reads $\mathcal{D} = 1/f$. Now, we get

$$\Delta\mathcal{D} = \frac{\partial\mathcal{D}}{\partial f}\Delta f = -\frac{1}{f^2}\Delta f \quad . \tag{S5.8}$$

Combining Eq. (S5.7) with Eq. (S5.8) and using $\Delta f = \pm\Delta z_f$ finally delivers

$$\Delta\mathcal{D} = \mp\frac{1}{f^2}\Delta z_f = \mp\frac{\lambda}{d^2_\mathrm{pupil}} \quad . \tag{S5.9}$$

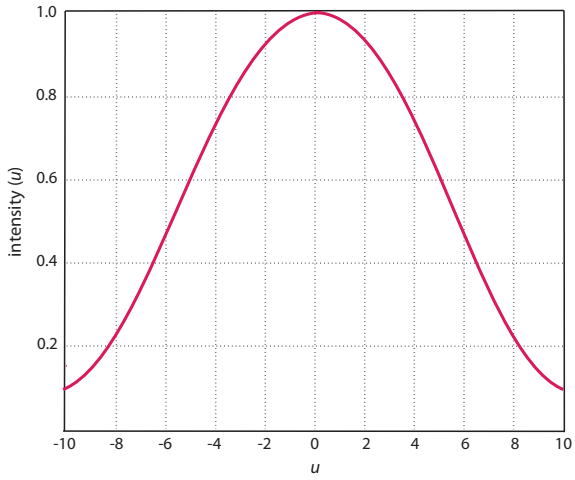

Figure S5.2 sinc^2(u) function

P5.2
Hartman-Shack wavefront sensor

1. The wavefront aberrations for defocus and spherical aberration at a wavelength of $\lambda = 550$ nm of a collimated beam with a diameter of 3 mm are to be measured with a Hartmann–Shack wavefront sensor. The CCD detector has a pixel size of 7 µm. With suitable algorithms, the centroid can be determined to within $1/20^{\text{th}}$ of a pixel. Which focal length should a microlens have to allow the determination of defocus as a Zernike coefficient down to $\lambda/20$. How accurately can the Zernike coefficient of the aperture error be determined for this focal length? What causes this difference?

2. If the finite size a of the detector elements is taken into consideration, then in the case of standard evaluation algorithms for the centroids, the dynamic range of the sensor is given by a spot leaving the surface assigned to the detector element on the sensor. In a simple geometric image, what is the extent of the maximal measurable defocus of the above sensor if $N = 30$ elements are assumed across the beam diameter and the fill factor is set to 1? If you assume that the lenses are diffraction-limited in the small elements, then finite-sized spots are obtained. What is the above-calculated maximal defocus when taking diffraction into consideration? Remember that the detector elements are squared (Figure 5.23).

3. Discuss the influence of different coherence states of the incident signal wave on the measuring result. What happens if the CCD sensor is positioned exactly in the focal plane of the microlens array? What is the effect of using various wavelengths? What happens at the edge of a sharply limited wave to the signal of partially illuminated detector elements? How can this problem be solved in practical applications if the intensity of the waves is constant?

Solution:

1. The wave aberration of the defocus in normalized coordinates is given by

$$\mathcal{W}_{\text{def}}(r) = c_2^0 \cdot (2r^2 - 1) \ ,$$

and the gradient of the wavefront is given by the corresponding derivative. In the Hartmann–Shack wavefront sensor, the inclination of the wavefront or the angle θ of the center of gravity beam in a sub-aperture is the decisive measure for the spot offset Δx. In this context, please refer to Figure S5.3. The direction of the normal line and/or the inclination of the wavefront is given by the derivative with respect to position, that is,

$$\frac{\mathrm{d}\mathcal{W}_{\text{def}}}{\mathrm{d}r} = 4r \cdot c_2^0 \ .$$

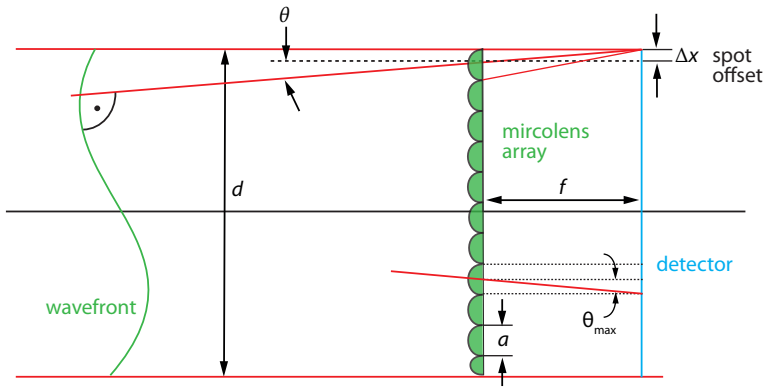

Figure S5.3 Optical arrangement of a Hartmann–Shack wavefront sensor.

This gradient has a maximal value at the edge (r = 1) determined by

$$\left.\frac{\mathrm{d}\mathcal{W}_{\mathrm{def}}}{\mathrm{d}r}\right|_{\mathrm{max}} = 4c_2^0 \ . \tag{S5.10}$$

In analogy, the aperture error is given by

$$\begin{aligned}
\mathcal{W}_{\mathrm{sph}}(r) &= c_4^0 \cdot (6r^4 - 6r^2 + 1) \ , \\
\frac{\mathrm{d}\mathcal{W}_{\mathrm{sph}}}{\mathrm{d}r} &= c_4^0 \cdot (24r^3 - 12r) \ , \\
\left.\frac{\mathrm{d}\mathcal{W}_{\mathrm{sph}}}{\mathrm{d}r}\right|_{\mathrm{max}} &= 12 \cdot c_4^0 \ .
\end{aligned} \tag{S5.11}$$

Let the center beam in the Hartmann–Shack sensor incline an angle θ with the optical axis. Assume the sub-apertures of diameter a to be small as compared to the diameter d. Then, at the edge of the sensor of beam diameter d, we have

$$\theta \approx \tan\theta = \frac{\Delta x}{f} = \frac{\lambda}{d/2} \cdot \left.\frac{\mathrm{d}\mathcal{W}_{\mathrm{def}}}{\mathrm{d}r}\right|_{\mathrm{max}} \ , \tag{S5.12}$$

where we used the spot offset Δx and sub-aperture lenses with a focal length f. Here, the pre-factor 2 λ/d comes into play as the wave aberration is normalized for λ in the Zernike representation in the pupil radius, that is, the beam radius is normalized to 1. The normalization is required in order to obtain absolute units.

Using the pixel size p = 7 µm, it follows that $\Delta x_{\mathrm{min}} = p/20$, and the focal length follows from Eqs. (S5.12) and (S5.10) as

$$f = \frac{\Delta x \cdot d}{2\lambda \cdot \left.\frac{\mathrm{d}\mathcal{W}_{\mathrm{def}}}{\mathrm{d}r}\right|_{\mathrm{max}}} = \frac{p \cdot d}{40 \cdot \lambda \cdot 4c_{2\ \mathrm{min}}^0} = 4.77\ \mathrm{mm} \ . \tag{S5.13}$$

Accordingly, the accuracy of the determination of the aperture error is

$$c_{4\,\mathrm{min}}^{0} = \frac{p \cdot d}{12 \cdot 40\lambda \cdot f} = 0.0167 = \frac{1}{60} \ .$$

As the wave surface of the spherical aberration has a 3-fold larger slope than the defocus error at the edge (also evident from a comparison of Eqs. (S5.10) and (S5.11)), the gradient-based measuring method used in the Hartmann–Shack sensor is more sensitive by the same factor.

2. If the number of sub-apertures is $N = 30$, their diameter is given by

$$a = \frac{d}{N} = 0.10 \text{ mm} \ .$$

The maximum measurable defocussing can be obtained from Eqs. (S5.10) and (S5.13) for $\Delta x = \frac{a}{2}$ as

$$c_{2\,\mathrm{max}}^{0} = \frac{a/2 \cdot d}{8\lambda f} = 14.2 \ . \tag{S5.14}$$

This corresponds to the angle θ_{max} in Figure S5.3. The numerical aperture of a sub-aperture is

$$\mathrm{NA} = \frac{a/2}{f} = 0.021$$

and, accordingly, the diameter of the point-spread function PSF (analogous to Airy, without the factor 1.22) for a square aperture is

$$d_{\mathrm{PSF}} = \frac{\lambda}{\mathrm{NA}} = 0.0262 \text{ mm} \ .$$

Correcting the maximum permissible offset of the spot in Eq. (S5.14) by this value, the maximal value of the measurable defocussing decreases to

$$c_{2\,\mathrm{max}}^{0} = \frac{(a/2 - d_{\mathrm{PSF}}) \cdot d}{8\lambda f} = 6.8 \ .$$

The reason for making this correction is that the solely geometrical consideration presented above "looks" at the centers of the spots only. However, the spots do in fact have a finite dimension due to diffraction and, for analysis of the centers of gravity, the spots must still be resolved. According to the Rayleigh criterion, they have a distance from each other that corresponds approximately to the Airy diameter.

3. When a coherent wave is incident on the wavefront sensor, each individual spot will be nearly diffraction-limited and has a corresponding diffraction structure. The pixel-related discrete representation of the sensor must be sufficiently small such that these intensity distributions can be recorded with sufficient accuracy and analyzed with regard to the center of gravity. If the incident light is partially

coherent, the individual spots are broadened and have a less fine structure due to diffraction on the edges of the sub-apertures. This reduces the dynamic range, but the analysis of the center of gravity tends to become more accurate and more robust. However, one needs to remember that partially coherent light does not have an unambiguous phase. Hence, in this case, the wavefront sensor measures a direction of the Poynting vector that is averaged over the sub-aperture and all spectral components.

If the sensor is not positioned exactly in the focal plane (Figure S5.3), the angle-position deviation relationship of the exact Fourier setup is disturbed. The analytical equations are then no longer exactly correct. However, since these are still used in the typical case, the procedure interprets the produced error as the defocussing portion of the incident wave. In accordance with Figure S5.4a, the deviations of the center of gravity normalize evenly and, in the ideal case, there is no interference with the higher-order aberration terms. According to Figure S5.4b, errors occur on the edges of partly illuminated sub-apertures.

If various wavelengths are to be processed simultaneously by the same sensor (e.g., white light), this means that we have a partly coherent beam. On the other hand, the chromatic longitudinal aberration of the array lenses leads to a small degree of defocussing in the wavefront sensor. However, according to the discussion presented above, there are no problems associated with this type of sensor except for edge effects and a small defocus error.

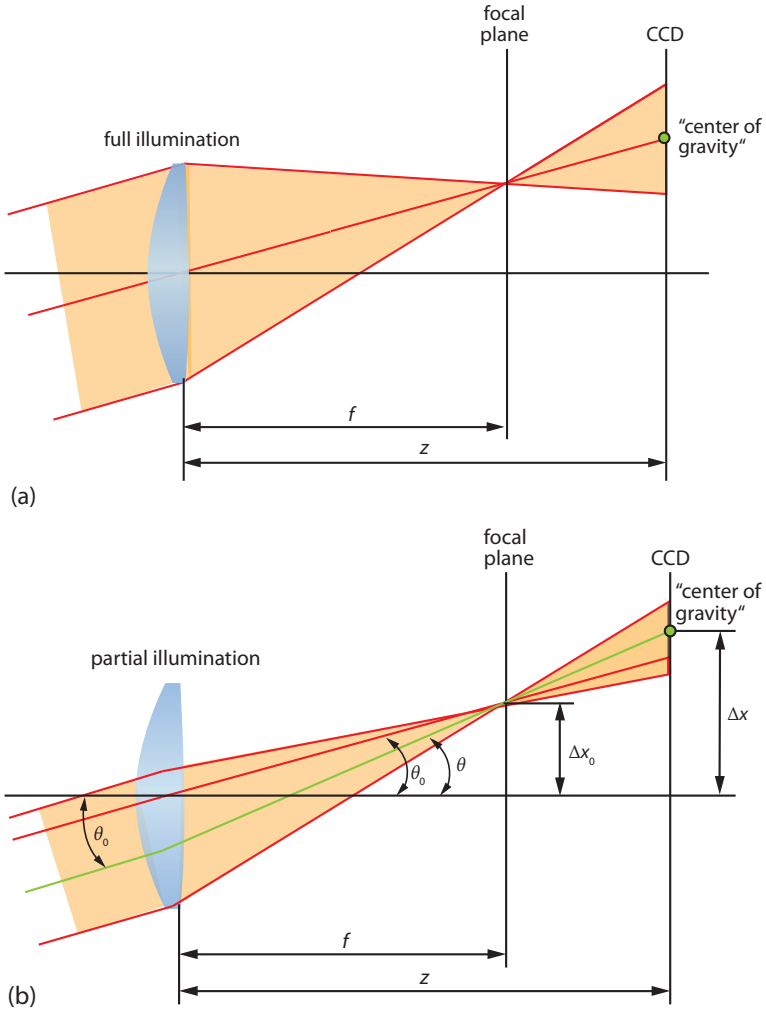

Figure 5.4 Even normalization of the deviations of the center of gravity.

P5.3
Aberrometry

Figure (5.28) shows the ocular wavefront table measurement as obtained by a ZEISS i.Profiler®plus. In the red box, the determined Zernike coefficients for an eye with a pupil diameter of $3.0\,\mathrm{mm}$ (analysis aperture) are listed in micrometer up to the order $n = 4$. On the left, the calculated metric values are shown:

1. Calculate the spherocylindric refraction values (polar notation) for a vertex distance of 12 mm.

2. Calculate the root mean square wavefront error $\mathrm{RMS}_{\mathrm{wfe}}$ for the lower-order aberration ($n = 2$), higher-order aberration ($n > 2$), and the total $\mathrm{RMS}_{\mathrm{wfe}}$.

Solution:

1. The spherocylindric refraction values (polar notation) are given by Eqs. (5.27) to (5.29), that is,

$$\mathrm{sph} = -\frac{4\sqrt{3}\,(c_2^0)}{r^2} + \frac{\mathrm{cyl}}{2}\ , \tag{5.27}$$

$$\mathrm{cyl} = -\frac{4\sqrt{6}\sqrt{(c_2^{-2})^{\,2} + (c_2^2)^{\,2}}}{r^2} + \frac{\mathrm{cyl}}{2}\ , \tag{5.28}$$

$$\mathrm{axis} = \frac{1}{2}\arctan\left(\frac{c_2^{-2}}{c_2^2}\right)\ . \tag{5.29}$$

From the screenshot (Figure 5.28), we can read

$$\begin{aligned} c_2^{-2} &= z(2,-2) = +0.05\ \mu\mathrm{m} \\ c_2^{2} &= z(2,+2) = -0.14\ \mu\mathrm{m} \\ c_2^{0} &= z(2,0) = +0.054\ \mu\mathrm{m} \end{aligned}$$

and $r = 1.5\,\mathrm{mm}$, which denotes the radius of the so-called analysis aperature. We then obtain

$$\begin{aligned} \mathrm{sph} &= 0.49\ \mathrm{D}\ , \\ \mathrm{cyl} &= -0.65\ \mathrm{D}\ , \\ \mathrm{axis} &= -9.8^\circ + 180^\circ \approx 170^\circ\ . \end{aligned}$$

These values actually refer to the plane of measurement of the aberrometer, that is, the entrance pupil of the patient located about 3 mm behind the corneal vertex.

If we want to calculate the sphero-cylindrical values for a correcting eyeglass in vertex distance (i.e., plane of the back vertex of the eyeglass), we can use

$$\mathcal{D}'_{\mathrm{v}}(L_{\mathrm{c2}}) = \frac{\mathcal{D}'_{\mathrm{v}}(L_{\mathrm{c1}})}{1 + \mathcal{D}'_{\mathrm{v}}(L_{\mathrm{c1}}) \cdot (L_{\mathrm{c2}} - L_{\mathrm{c1}})} \tag{5.36}$$

in which $L_{\mathrm{c1}} = 0.003\,\mathrm{m}$, $L_{\mathrm{c2}} = 0.012\,\mathrm{m}$, and $\mathcal{D}'_{\mathrm{v}}(L_{\mathrm{c1}}) = \mathrm{sph} = 0.49\,\mathrm{D}$. However, because of the relatively small sphero-cylindrical refraction values, the correction coming from Eq. (5.36) is negligible in this case.

2. According to Eq. (5.22), the root mean square wavefront error can be calculated via

$$\mathrm{RMS}_{\mathrm{wfe}} = \sqrt{\sum_{n>1,m} (c_n^m)^2} \ .$$

Although Eqs. (5.22) and (5.23) use c_n^m with two indices instead of c_j with one index, a sum of c_n^m is equivalent to a sum of c_j. Hence, we have

$$\sum_{n>1,m} c_n^m = \sum_j c_j \ .$$

The transform between m, n and j is based on Eq. (5.20) (see also Table A3) and given by

$$j = \frac{n^2 + 2n + m}{2} \ .$$

j	0	1	2	3	4	5	6	7	8
n	0	1	1	2	2	2	3	3	3
m	0	-1	1	-2	0	2	-3	-1	1
c_{j} (µm)		-		0.050	-0.054	-0.140	-0.029	-0.001	-0.040

With the results above and the definitions of Table A3, we can calculate the RMS of the lower-order aberrations (LOA) ($j = 3...5$) via

$$\mathrm{RMS}_{\mathrm{wfe}}\ (\mathrm{LOA}) = \sqrt{\sum_{j=3}^{5} (c_j)^2}$$
$$= \left(\sqrt{(0.050)^2 + (-0.054) + (-0.140)^2}\right)\ \mu\mathrm{m} = 0.016\ \mu\mathrm{m} \ .$$

The RMS of the higher-order aberrations (HOA) ($j = 6...14$) follows as

$$\mathrm{RMS}_{\mathrm{wfe}}\ (\mathrm{HOA}) = \sqrt{\sum_{j=6}^{14} (c_j)^2}$$
$$= \left(\sqrt{(-0.029)^2 + (-0.001)^2 + (-0.040)^2 + (0.011)^2 + ...}\right)\ \mu\mathrm{m} = 0.05\ \mu\mathrm{m} \ .$$

The total wavefront error is given by (j = 3 ... 14)

$$\mathrm{RMS}_{\mathrm{wfe,tot}} = \sqrt{\sum_{j=3}^{14} (c_j)^2} = 0.17\mu\mathrm{m} \ .$$

The result shows that the major contribution to the RMS of the wavefront error stems from lower-order aberrations.